Hydrothermal waves in Marangoni convection in a cylindrical container

A. B. Ezersky,* A. Garcimartín,† J. Burguete, H. L. Mancini,‡ and C. Pérez-García§
Departamento de Física y Matemática Aplicada, Facultad de Ciencias, Universidad de Navarra, 31080 Pamplona, Navarra, Spain
(Received 5 August 1992)

The features of hydrothermal waves that appear when a liquid layer is laterally heated are presented. A bifurcation is observed from a steady regime to a regime of a basic flow with superimposed traveling waves. Measured characteristics of waves are shown and compared with some recent theoretical predictions.

PACS number(s): 47.20.Dr, 47.35.+i, 44.25.+f

I. INTRODUCTION

Many situations are found in convection processes where the heating is not homogeneous. This is the case in different techniques, such as manufacturing of crystals using the float-zone method or laser welding. The heating is concentrated in some zones, and even for small temperature differences large-scale fluid motion arises as a consequence of convection. If temperature is increased, this large-scale flow loses stability and new types of motion (propagating waves) can appear.

The appearance of such waves has been predicted theoretically in previous works [1–3]. An oscillatory regime with a rotating structure has recently been observed [4] in a cylindrical container where the liquid, with a free surface, is heated from the axis, but propagating waves did not appear in that case. Several experiments have been performed on liquids with low Prandtl (Pr) numbers (see [5] and references in [6]), but it is difficult in those cases to quantify the parameters of the waves. In another paper [7], there is an indication that this kind of hydrothermal wave with high Pr fluids can appear in a cylindrical container heated only in the center, but no characterization of the waves was made. In the heated region, convective cellular motion can be observed (this is equivalent to a small aspect ratio convective cell). In the outer region (not heated from below) some waves were visible. Flow was visualized using aluminum powder, but quantitative measurements on the waves were not carried out. To our knowledge no experimental work giving the instability thresholds and wave parameters (such as frequency and velocities) has yet been reported. In this work we present evidences of hydrothermal waves and values for their basic features. In Sec. II we describe the experimental setup and the measurement techniques. Section III is devoted to a brief review of some previous theoretical results on the main mechanisms and parameters of the phenomena. We gather our results in Sec. IV. Finally, some conclusions are given in Sec. V.

II. EXPERIMENTAL PROCEDURES

The convective container is represented in Fig. 1. It is made of a single round piece of Delrin in which a hole was machined to harbor a copper cylinder. This cylinder was heated by means of a power-regulated electric resistor. The bottom of the copper cylinder is covered with isolating material to avoid losses as much as possible. Two thermocouples are placed in it, one in the metal below the heated region and another in the lateral wall of the container. This yields the temperature difference responsible for this instability. Refrigerating the upper air layer does not noticeably change wave features, and so we went without it in order to have better shadowgraph images. In fact, it has been stated [5] that, being that the heat exchange to the air is small compared to the lateral heat transport, the vertical temperature difference is only relevant to establish the basic flow, but has little influence on the waves. Therefore our system is equivalent to a lateral heating convective device, where the central part acts as a hot source and the liquid, after losing heat to the air, arrives to the wall and a return flow is established.

The employed liquids are silicone oils whose properties are listed in Table I. Liquid depth could be varied from 2 to 8 mm. In each run the same procedures are followed to ensure repeatability. We first heated the central part to a fixed temperature. The heater is then switched off and images are recorded along with temperatures. Afterwards we chose several points to study the properties of the waves. This can be done in this way because the characteristic time of cooling is much larger than the characteristic time of the unsteady processes observed in the system (several hours versus seconds). Temperature precision is of about 0.1 °C, which corresponds to its variation during each record.

One useful method to visualize fluid motions is to seed

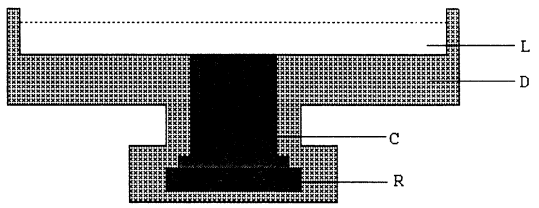

FIG. 1. Sketch of the container used in the experiments: *D*, piece of Delrin; *R*, electrical resistor embedded in isolant; *C*, copper; *L*, liquid under test. The drawing is simplified and not to scale. The inner diameter of the cavity containing the liquid is 100 mm.

TABLE I. Properties of 5-cS polydimethylsiloxane (silicone oil) at different temperatures: density, shear viscosity, kinematic viscosity, surface-tension coefficient, specific heat at constant pressure and volume, thermal conductivity, and thermal diffusivity.

T (K)	ρ (g/cm^3)	μ (cP)	ν (cS)	σ (dyn/cm)	c_p (cal/g °C)	c_v (cal/g °C)	λ (W/m K)	κ (10^2 cm^2/s)
288	0.917	4.95	5.40	18.00	1.623	1.326	0.1375	0.1101
293	0.913	4.63	5.07	17.50	1.631	1.373	0.1372	0.1094
298	0.908	4.16	4.58	17.20	1.638	1.383	0.1369	0.1088
303	0.903	3.78	4.18	16.40	1.647	1.397	0.1366	0.1082
308	0.899	3.49	3.88	16.20	1.656	1.409	0.1363	0.1076
313	0.895	3.26	3.64	15.90	1.666	1.423	0.1360	0.1069
318	0.889	3.04	3.42	15.40	1.666	1.436	0.1357	0.1063
328	0.881	2.65	3.01	14.70	1.676	1.463	0.1351	0.1051

aluminum powder in the fluid, as has been done in previous works [7,8], because the main fluid properties, such as thermal conductivity and kinematic viscosity, are changed only a small amount. But it is clearly more indicated to use a noninvasive method to observe waves, where inertial properties can be more relevant and nontrivially related to the velocity field. This is accomplished with optical methods of flow visualization [9]. We have arranged a shadowgraph system that allows sharp visualization of surface waves. The setup is sketched in Fig. 2. Light from a point source located at the focus is directed onto a spherical mirror which reflects plane waves towards the surface of the liquid. Light is partially reflected back to the mirror and refocused through a beam splitter onto the detection system. In order to match the dimensions of the image of the cell to the charge-coupled-device (CCD) detector, we used a photographic teleobjective that along with the mirror forms a telescope. Small deviations from flatness in the surface of the liquid can be visualized as bright or dark zones, depending on whether the surface is concave or convex. If a knife edge is placed at the focus, the system is transformed into a schlieren setup [9]. In order to monitor, store, and process the images we connected the CCD camera to a computer, which in turn was connected to a standard video cassette recorder to allow convenient recording of the images. To obtain better resolution images we took some photographs with the same setup. All was placed on a vibration-isolated table.

III. SOME THEORETICAL TOOLS

A liquid layer open to the air can develop convection under a lateral temperature gradient due to the Marangoni effect (the variation of the surface tension with temperature leads to stresses that induce global motions in the fluid). Though there are papers (see [1] for a review) in the literature covering numerical simulations of Marangoni convection with horizontal temperature gradient, theoretical investigation of hydrothermal wave instability has been carried out mainly for pure Marangoni convection and for a two-dimensional flow. We nevertheless recall here the most significant results [1–3] for the sake of comparison. In [2] a linear stability analysis is performed for a rectangular box of infinite length. It must be emphasized that our geometry is different from that considered there, but we will try to understand our observations following the analysis in these papers. Because of this we can only rely on them as an approximation to our case.

According to [1], the surface velocity U_s induced by the Marangoni effect is:

$$U_s = \frac{1}{4}\frac{\frac{d\sigma}{dT}\frac{dT}{dx}d}{\mu} ,$$

where $d\sigma/dT$ is the coefficient of variation of surface tension with temperature, dT/dx is the horizontal temperature gradient (assumed to be constant), d is the

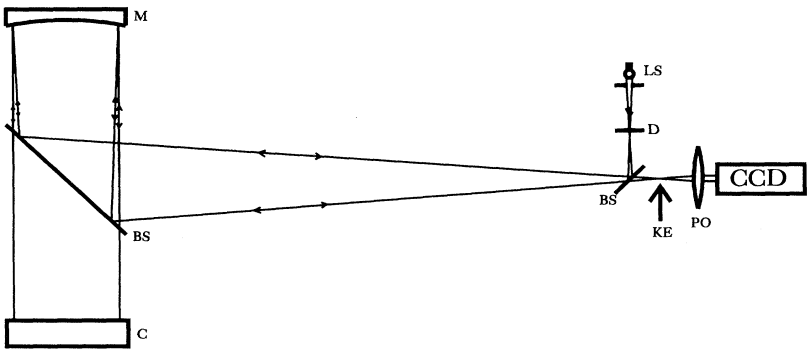

FIG. 2. Sketch of the experimental setup: LS, light source; D, diaphragm; BS, beam splitter; M, mirror; C, container; KE, knife edge; PO, photographic objective; CCD, standard CCD camera. The system was made slightly astigmatic (less than 5°) to avoid the direct light. The focal length of the spherical mirror is about 1.5 m.

depth, and μ is the viscosity. (We take this formula as a rough estimation; the temperature profile is not linear in the experiment.)

Critical temperature difference ΔT_{crit} for the appearance of waves is also provided in those papers. For high Pr the critical Marangoni number (M) is close to 400. We have a lateral temperature gradient; the formula for the critical M is then

$$M_c = \frac{\frac{d\sigma}{dT}\frac{dT}{dx}d^2\text{Pr}\rho}{\mu^2} ,$$

where ρ is the density.

A rough estimation of the temperature gradient can be obtained by calculating $(T_h - T_w)/r$, where T_h is the temperature of the heater, T_w is the temperature of the sidewall, and r is the radius. On the plane d versus $T_h - T_w$ the critical line is given approximately by the expression (buoyancy has been neglected)

$$T_h - T_w = \frac{M_c \mu^2 r}{d^2 \text{Pr}\rho \frac{d\sigma}{dT}} .$$

The critical wave number of unstable waves has been determined from the linear analysis in [2]. For the liquid used in the experiments Pr can be considered to be infinite. In this case the value obtained in [3] at the onset of instability is approximately $k = 2.4$ in nondimensional units.

IV. EXPERIMENTAL RESULTS

Spatial bifurcations observed in our system depend on liquid depth and on whether the temperature difference between the heated region and the lateral walls is increased or decreased. A description of what is going on in the heated region can be found in [7]. Here we will focus on the outer, inhomogeneously heated region.

For small liquid depth (less than 0.3 cm) we observed the following spatial bifurcations as we increase temperature difference. First of all, the convective regime appears. Convection in inhomogeneously heated liquids is characterized by one toroidal vortex in the container connecting the heated region with the sidewall. The first transition takes place when several stationary concentric rolls are developed surrounding the heated region. Heat is then transported by these rolls from the heated region outwards. In the heated region, there is also a bifurcation from steady to nonsteady convection. Perturbations arising from nonsteady convection affect the structure of convective rolls and cause numerous defects. In the outer region there is another transition when the structure of rolls fails to cope with heat transport requirements and waves appear superimposed on the basic flow. The physical mechanism responsible for these waves is the surface-tension dependence on temperature. In most liquids surface tension decreases when temperature increases. If we consider a hot spot in the surface of the liquid, the surface tension of the surroundings (which will be largest where the surface is coldest) will pull it. Then

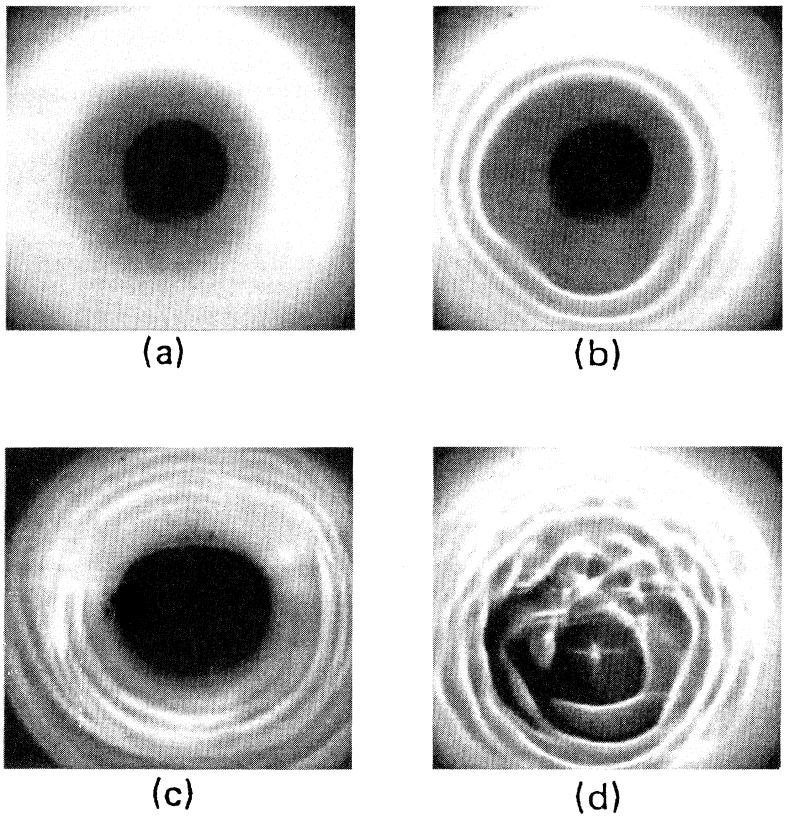

FIG. 3. Sequence of bifurcations for small depth: (a) steady state; (b) concentric rolls; (c) thermocapillary waves; (d) the same waves with nonsteady convection in the heated region.

the hot spot will move away, thus forming a sustained instability.

It must be noted that the appearance of propagating waves is not directly related to nonsteady convection in the heated region. To test this we performed a control experiment putting a metal cylinder on the heater that replaces the fluid in the central zone. By doing that we effectively suppressed the convection there. The same bifurcation sequence can then be observed. That sequence is shown in Fig. 3. Figure 3(a) shows the steady convection state, Fig. 3(b) shows the structure of concentric rolls, and in Fig. 3(c) waves can be seen propagation from the center to the periphery. If the cylinder is removed, waves become less correlated in the azimuthal direction, much in the same way that the structure of rolls is perturbed by nonsteady convection, but their features (frequency, velocity) do not seem to change. Figure 3(d) shows nonsteady convection in the heated region and waves propagating from there to the walls of the container. We also observe some sort of hysteresis: when the system is cooled, no concentric rings appeared for small temperature differences.

In liquids with larger depth (more than 0.3 cm), we do not observe concentric rolls. During the heating there was a transition from the toroidal vortex to traveling waves, and the inverse during cooling, the latter again taking place at another temperature difference. It must be pointed out that the reason for this hysteresis can be a different temperature distribution at the bottom of the container or differences in the liquid temperature. This particular point has not been checked.

To measure wave properties we grabbed a line of pixels from the image, in the radius range of the container where waves were observed, at regular intervals, thus constructing an image whose axes represent radius and time (Fig. 4). Time intervals between two consecutive lines were typically of 100 ms. In this way the wave appears as a dark line whose slope is the velocity. Knowing the number of recorded lines, the timing, and the length of the recorded segment, one can readily obtain a quantitative velocity measurement. Spatial and time frequencies can be obtained by means of a Fourier transform of the image in the vertical and the horizontal directions, respectively. As wavelength clearly changes with radius, it is more accurate to take just one vertical (horizontal) line instead of the entire image.

Quantitative measurements were made only when cooling. Proceeding in the way explained above, we established wave frequency and velocity dependencies on temperature difference and depth of the liquid. For large temperature difference (for large we mean $\Delta T > 25\,^{\circ}\mathrm{C}$), the smaller the depth the higher the frequency, while for low ΔT the case is the reverse (in Fig. 5 frequency is plotted for low ΔT). This may be connected with different contributions of nonsteady convection and hydrothermal instability to the generation of waves.

For large ΔT we had numerous thermal plumes in the heated region. Perturbations caused by these plumes are transformed into propagating waves a distance away from them. Wave frequencies are seemingly determined by the characteristic time of the oscillation of the plumes,

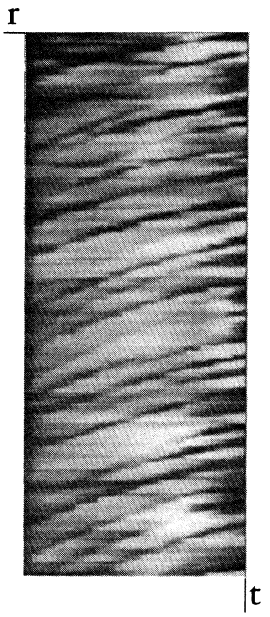

FIG. 4. Result of grabbing one line of pixels along the radius; the center of the container is situated on the right side and the wall on the left side. Waves can be seen as dark stripes.

which is greater if d is smaller. We believe this to be the reason for the described behavior at large ΔT.

For small ΔT thermal plumes were not observed at all and wave frequency depends on departure from critical ΔT, which is smaller for small d. It must be noted that for ΔT very near critical values we observed intermittency in the generation of waves. One wave train propagated from time to time with nonhomogeneous amplitude in

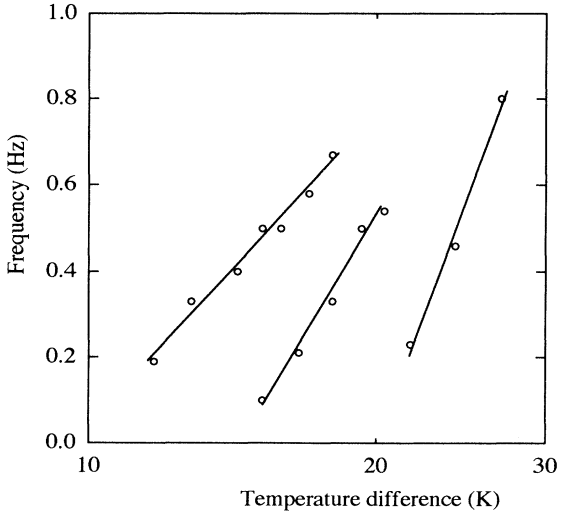

FIG. 5. Frequency of waves as a function of ΔT for different depths: from left to right, $d = 0.38$, 0.32, and 0.23 cm, fitted for low values of ε to find ΔT_{crit}. A logarithmic scale has been used for ΔT.

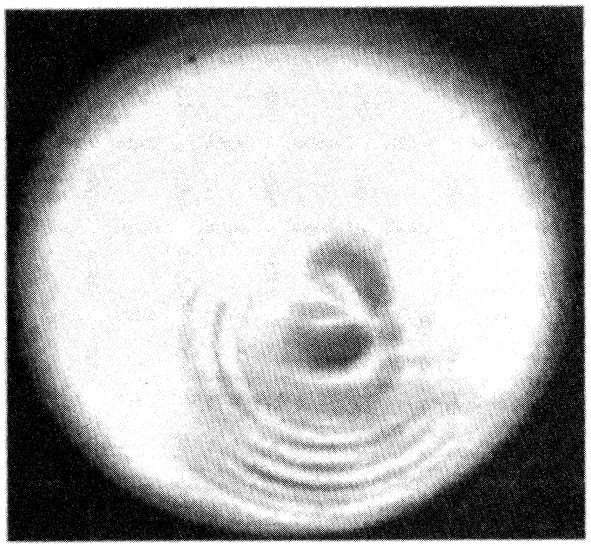

FIG. 6. Wave train observed at the onset of hydrothermal wave instability.

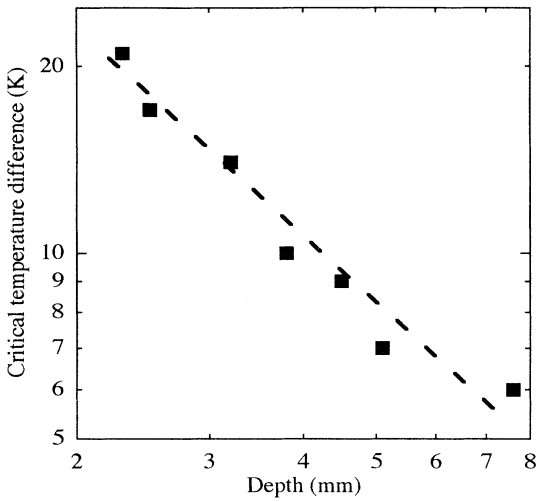

FIG. 7. Log-log plot showing ΔT_{crit} for different depths (squares) fitted with a dashed line.

the azimuthal direction (see Fig. 6). In those cases we did not measure wave frequency strictly speaking, which would be the frequency inside one wave train, but an averaged frequency (number of waves divided by time) over a period larger than typical time between wave trains. For ΔT moderately higher waves were generated almost continuously. It is known [10] that near the onset of an oscillatory instability frequency is expected to behave as the square root of criticality, defined in our case as $\epsilon=(\Delta T-\Delta T_{crit})/\Delta T_{crit}$. By fitting the dependency of frequency on ΔT (Fig. 5), we extrapolate it to determine the threshold ΔT_{crit} that marks the onset of waves. This we show in Fig. 7. Experimental and theoretical results are close, but the agreement is better in the case of smaller depths. We believe buoyancy to play a stabilizing role for large d.

Wave phase velocity changes with radius as can be readily seen in Fig. 4. We measured mean wave velocities to compare different cases. The velocity dependence on d and ΔT is shown in Fig. 8. Velocity grows with ΔT and also shows a growing tendency with d. These values can be compared with the surface velocity. Estimated calculations of surface velocities are shown in Fig. 8 along with experimental results. It is worth noting that the calculated surface velocity is larger than the velocity of the waves observed in the experiment, a situation typical in hydrodynamical instabilities: when a system loses stability and waves appear, their phase velocity is smaller than the maximum velocity of the flow and larger than the minimum velocity. One would be tempted to think that the velocity of the waves for different liquid depths should be proportional to the surface velocity, because velocity profiles are similar for Marangoni-driven convection. Nevertheless, Fig. 8 shows that this is not the case; the discrepancies between experimental and theoretical values increases when d increases. This could be due to buoyancy effects that become more significant with thick layers.

There are two difficulties for estimating the wave number, namely (i) the aspect ratio of our system is relatively small (just several wavelengths) and (ii) k changes with distance from the center of the cavity. Nevertheless we can estimate an averaged k near the onset of the instability in two ways: (1) by measuring the spatial period in every wave train, and (2) by estimating it as $k_{av}=(2\pi d/V)f$, where V is the wave velocity and f stands for the averaged frequency. For an ϵ of about 0.3 we measured k_{av} to be 2.9 ± 0.3 following the first method; this is in fair agreement with the value for k_{av} provided in [3]. The second method gives $k_{av}=2.4$ for $d=0.25$ cm and $k_{av}=3.1$ for $d=0.5$ cm for the same ϵ.

The main difference between the features of the waves we have observed and the predicted is the following. According to [1–3] the waves should propagate upflow, with smaller velocity than U_s. Wave velocity in our experiment is smaller than the velocity theoretically estimated for the flow near the surface (see Fig. 8), but the waves travel in the same direction than the flow on the surface. We should mention here that in the case of 5-cS silicone oil buoyancy and surface-tension effects are of the same order for a liquid depth $d=\sqrt{(d\sigma/dT)/\rho g\alpha}\cong 3$ mm, where σ is the surface-tension coefficient, ρ is the density, and α is the thermal expansion coefficient. In our experiments the depth was 2 mm $< d <$ 8 mm, and so buoyancy cannot be neglected. In [1–3] buoyancy is not taken into account. In Ref. [6] buoyancy is taken into consideration and waves propagate downward, i.e., in the same direction than the flow on the surface. One could rely on this to suggest that the effect of buoyancy may explain why we do observe downward propagation. Nevertheless, results obtained in Ref. [6] assume low Pr while we have worked with large Pr fluids, and in many of the calculations performed negative Re have been assumed (which means $d\sigma/dT>0$).

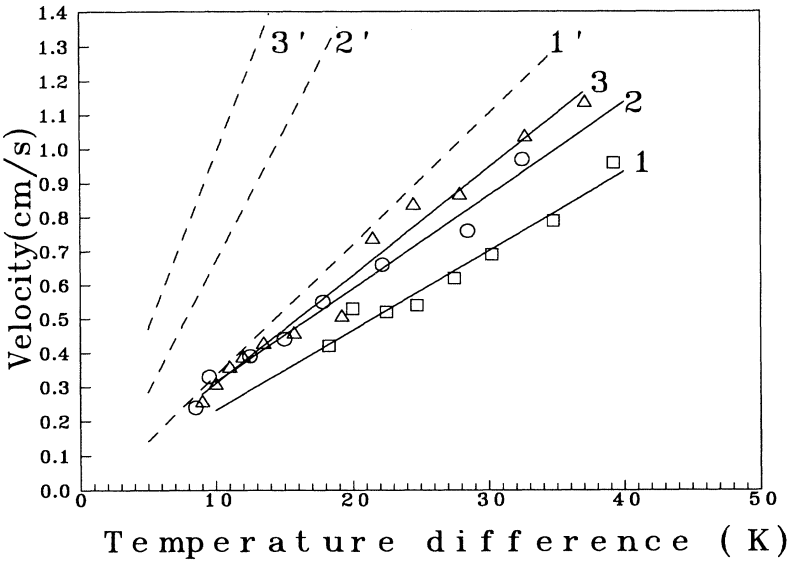

FIG. 8. Velocity of waves vs ΔT for different depths: 1, $d=0.26$ cm; 2, $d=0.51$ cm; 3, $d=0.76$ cm. Dashed lines 1', 2', and 3' represent the surface velocity predicted for those depths in [1–3].

Anyway, the direction of propagation of waves may be connected with the large-scale velocity profile. In [1–3] viscosity dependence on temperature is not taken into account. But in our experiment viscosity indeed changes with temperature, thus altering the mean profile and the location of the critical layer for hydrothermal waves. A small displacement in the location of the critical layer can indeed have drastic consequences in the direction of propagation of hydrothermal waves if it is situated near $U(z)=0$ [$U(z)$ is the velocity profile along the vertical coordinate].

V. CONCLUSIONS

In this work we have shown the existence of hydrothermal wave instability which arises in Bénard-Marangoni convection with lateral heating. Temperature threshold measurements for such instability as well as frequency and wave velocity behavior for different depths and temperature differences are given. Results are found to agree qualitatively with previous theoretical works but the direction of propagation of waves for large depths is in contradiction with that predicted. This fact needs further explanation.

ACKNOWLEDGMENTS

We want to thank R. Gilmore (Philadelphia, PA) for useful suggestions and comments. We are also indebted to Dr. G. B. Mindlin, Dr. T. Ondarçuhu, and P. Elizalde for their helping and discussions. The properties of the silicone oils employed were measured at the laboratory of I. B. Rabinovich (Institute of Chemistry, Nizhny Novgorod University, Nizhny Novgorod, Russia). This work has been partially supported by DGICYT (Spanish Government) through Contract Nos. OP90-0098 and PB91-0627, and by the Gobierno de Navarra (OF 725/91). Two of us (A. B. E. and H. L. M.) also acknowledge DGICYT for financial support.

*Permanent address: Institute for Applied Physics, Russian Academy of Sciences, Nizhny Novgorod, Russia.
†Author to whom all the correspondence should be addressed.
‡Also at CITEFA/CONICET (1603 Villa Martelli) and Universidad de San Luis, Chacabuco y Pedernera, 5700 San Luis, Argentina.
§Also at Departament de Física Fonamental, Facultat de Ciències Físiques, Universitat de Barcelona, Avgda. Diagonal 647, 08028 Barcelona, Catalonia, Spain.

[1] S. H. Davis, Annu. Rev. Fluid Mech. **19**, 403 (1987).
[2] M. K. Smith and S. H. Davis, J. Fluid Mech. **132**, 119 (1983).
[3] M. K. Smith, J. Fluid Mech. **194**, 391 (1988).
[4] Y. Kamotani, J. H. Lee, S. Ostrach, and A. Pline, Phys. Fluids A **4**, 955 (1992).
[5] S. Ostrach, Y. Kamotani, and C. L. Lai, Physiochem. Hydrodyn, **6**, 585 (1985).
[6] H. Ben Hadid and B. Roux, J. Fluid Mech. **235**, 1 (1992).
[7] O. V. Vashkevisch, A. V. Gaponov-Grechov, A. B. Ezersky, and M. I. Rabinovich, Dokl. Akad. Nauk **293**, 571 (1987) [Sov. Phys. Dokl. **32**, 197 (1987)].
[8] E. L. Koschmieder and S. A. Prahl, J. Fluid Mech. **215**, 571 (1990).
[9] W. Merzkirch, *Flow Visualization* (Academic, London, 1987).
[10] R. Gilmore, *Catastrophe Theory for Scientists and Engineers* (Wiley, New York, 1981).

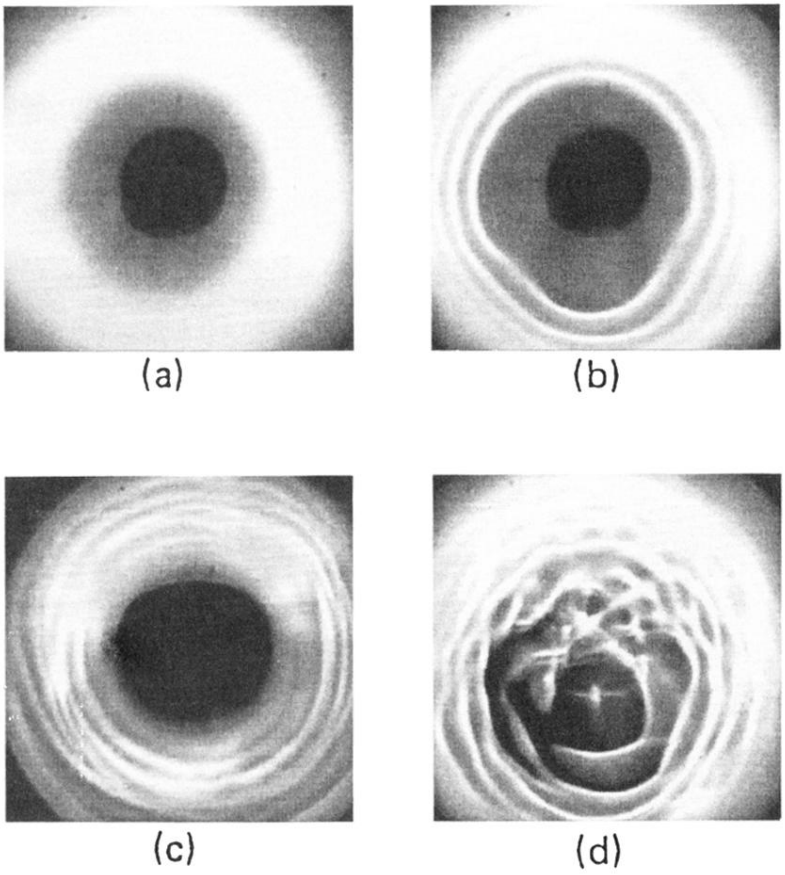

FIG. 3. Sequence of bifurcations for small depth: (a) steady state; (b) concentric rolls; (c) thermocapillary waves; (d) the same waves with nonsteady convection in the heated region.

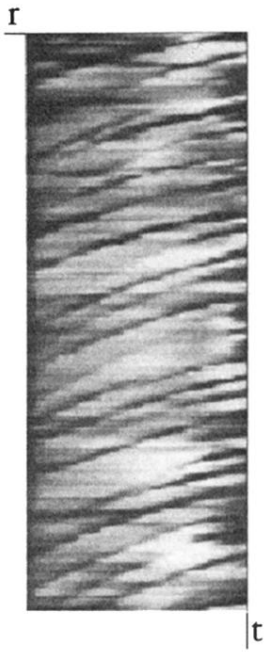

FIG. 4. Result of grabbing one line of pixels along the radius; the center of the container is situated on the right side and the wall on the left side. Waves can be seen as dark stripes.

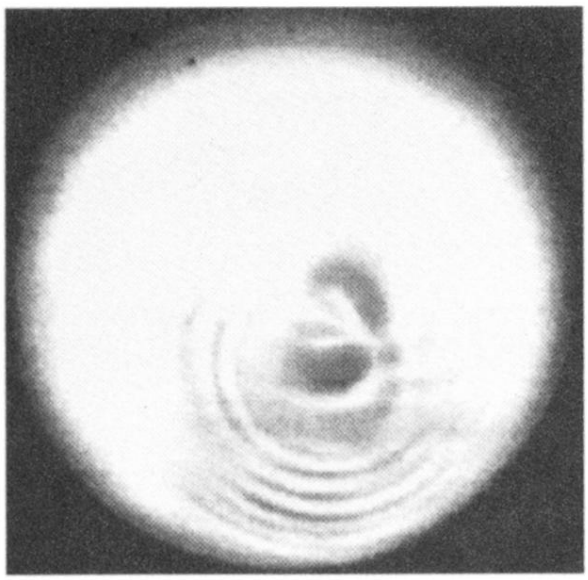

FIG. 6. Wave train observed at the onset of hydrothermal wave instability.